

## CHARACTERISTICS OF INVERTER-FED ULTRASONIC MOTORS – OPTIMIZATION OF STATOR/ROTOR-INTERFACE

J. Maas, P. Ide, H. Grotstollen

Institute for Power Electronics and Electrical Drives, FB14 - LEA  
University of Paderborn, Germany

### Abstract:

The stator/rotor-interface of rotary travelling wave ultrasonic motors is modelled for the general case of non-ideal waves. For optimization of drives performance the resulting speed-torque characteristics as well as the efficiency are analysed in detail by simulation and verified by measurements on a prototype drive. As a result it is proved that an optimized operation mode is obtained only, if an ideal wave is generated. Further investigations concern on an optimal choice of the applied axial force of the interface for maximum output power or best power/efficiency-performance.

### Introduction

Piezoelectric ultrasonic motors (USMs), in particular rotary travelling wave type USMs, show high torque densities at low rotational speed and are more compact than conventional electromechanical geared motors. Thus, USMs have attracted considerable attention as new actuators. In a travelling wave type USM two orthogonal vibration modes are excited to resonance by a piezoelectric ceramic. Due to the travelling wave the surface points of the stator perform elliptic motions driving the rotor by frictional force [1]. The electrical excitation of motor vibrations is mostly applied by a resonant converter [3]. Due to the inherent nonlinear characteristic of USMs, theoretical modelling requires intensive efforts, but it is indispensable for drives optimization by simulation. Therefore, the total electromechanical system of travelling wave USMs powered by a resonant converter is modelled [4]. Especially, the torque generation and reactions on the stator caused by the contact forces are derived describing the general case of non-ideal travelling waves.

The objective of this paper is to outline a framework for optimization of the stator/rotor-interface. The influences of well defined modal amplitudes and different axial forces, usually applied by a disc spring, are investigated from a theoretical and a practical point of view. After a brief review of modelling the stator/rotor-contact by an elastic contact model, the speed-torque characteristics as well as the efficiency are analysed in detail and verified by measurements on a prototype drive. Finally, a design procedure for optimization of the stator/rotor-interface is presented involving optimization methods for maximum output power or best power/efficiency-performance.

### Modelling of Stator/Rotor-Contact Interface

For modelling the stator's vibration a two-mode approximation describing the n-th eigenmode by

$$w_1(\hat{x}, t) = w_{1,t} \cdot \sin k\hat{x} \quad (\text{sine-mode}), \quad (1)$$

$$w_2(\hat{x}, t) = w_{2,t} \cdot \cos k\hat{x} \quad (\text{cosine-mode}) \quad (2)$$

is assumed, with  $w_{1,t}$  and  $w_{2,t}$ , the modal amplitudes and  $k = 2\pi/\lambda$ , where  $\lambda$  is the wavelength of the n-th mode. After superimposing both standing waves and introducing a wave oriented coordinate system rotating with the travelling wave [4] we obtain:

$$w(x, t) = \sqrt{w_{1,t}^2 + w_{2,t}^2} \cdot \cos kx = \hat{w}(t) \cdot \cos kx \quad (3)$$

as general case for a non-ideal travelling wave. In addition the horizontal velocity of the stator's surface points is necessary [2], which is given by

$$v_h(x, t) = d_{sp} \cdot \frac{ak\sqrt{\dot{w}_{1,t}^2 + \dot{w}_{2,t}^2}}{\hat{v}_h(t)} \cdot \cos(kx + kx_c), \quad (4)$$

$$\text{with } kx_c = \text{atan} \frac{w_{1,t}\dot{w}_{1,t} + w_{2,t}\dot{w}_{2,t}}{w_{2,t}\dot{w}_{1,t} - w_{1,t}\dot{w}_{2,t}}. \quad (5)$$

$kx_c$  is the phase shift between the waves of vertical displacement and horizontal velocity.  $d_{sp}$  is the actual direction of the surface points calculated by the negative sign of the denominator of (5), [4].

The contact mechanism of non-ideal travelling waves (eqn. (3) and (4)) is illustrated for an arbitrary moment in Fig. 1, [4]. The stator is assumed to be rigid while

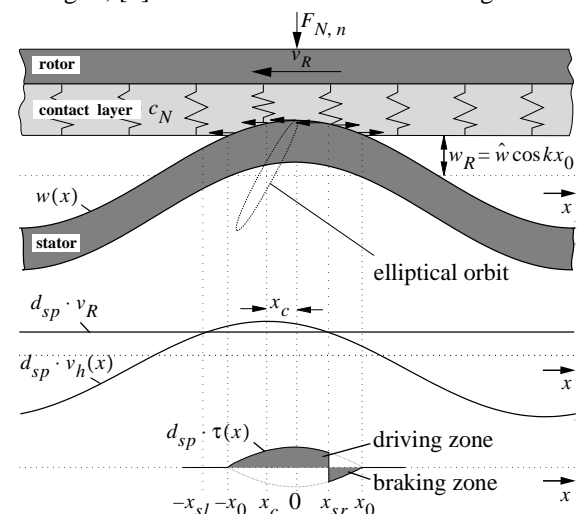


**Fig.1:** Stator/rotor-contact for non-ideal travelling waves. The displacement  $x_c$  is unequal to zero in general and causes unsymmetrical contact mecha-

the elastic contact layer of the rotor is modelled as linear spring with equivalent stiffness  $c_N$ . The overlap between rotor and stator is defined by  $\hat{w} \cos kx - w_R$ , resulting in a normal contact pressure distribution

$$p(x) = c_N(\hat{w} \cos kx - w_R) \quad (6)$$

along the contact region  $-x_0 \leq x \leq x_0$ . The state quantity  $w_R = \hat{w} \cos kx_0$  models the separation between the stator surface at  $w = 0$  and the undeformed contact layer. Coulombs' friction law is assumed modelling only slip effects by the coefficient  $\mu$ . Thus, the tangential stress  $\tau(x)$  along the contact region is calculated by

$$\tau(x) = d_{sp} \cdot \text{sgn}(\hat{v}_h(t) \cdot \cos(kx + kx_c) - d_{sp} v_R) \cdot \mu \cdot p(x) \quad (7)$$

At the stick points  $x_{sl}$  and  $x_{sr}$  ( $x_{sl}, x_{sr} \leq x_0$ ) a sudden alteration of the tangential stress from driving force to braking force or reverse occurs related to the tangential velocity  $v_h$  and to the velocity of the rotor  $v_R$  at contact radius  $r = R_w$ . The torque is determined by integrating  $\tau(x)$  over the contact zone and multiplying with  $R_w$  and  $n$ , the number of wave hills:

$$M_R = R_w \cdot n \int_{-x_0}^{x_0} \tau(x) dx \quad (8)$$

In dealing with the dynamics of the rotor, two degrees of freedom must be taken into account: First the axial motion and second the rotation of the rotor. The dynamics of the axial rotor motion (Fig. 1) is obtained through the force equilibrium in  $z$  direction:

$$m_R \ddot{w}_R + d_Z \dot{w}_R = \underbrace{n \int_{-x_0}^{x_0} p(x) dx}_{F_{Rz}} - F_N, \quad (9)$$

with  $m_R$ , the mass of the rotor,  $d_Z$ , an appropriate damping term and  $F_N$ , the applied axial force.

The equation of rotational motion is calculated by

$$J \dot{\omega}_R = M_R - M_L, \quad (10)$$

where  $M_L$  is the applied torque and  $J$  represents the drive's inertia. The rotor velocity  $v_R$  equals  $\omega_R R_w$ .

In order to determine the efficiency of the stator/rotor-contact  $\eta_{S/R}$  at steady state the following ratio of mechanical output to input power has to be evaluated by time averaging:

$$\eta_{S/R} = \frac{\int_0^{T_S} M_R(t) \omega_R(t) \cdot dt}{\int_0^{T_S} (p_n(t) + p_t(t)) dt} \cong \frac{M_L \cdot \int_0^{T_S} \omega_R(t) dt}{\int_0^{T_S} p_t(t) dt}, \quad (11)$$

whereby  $T_S = 1/f_S = 2\pi/\omega_S$  denotes the reciprocal of the feeding frequency  $f_S$ ,  $p_n$  models the negligible losses of axial rotor motion and  $p_t$  describes the tangential input power, which is calculated by:

$$p_t = n \int_{-x_0}^{x_0} v_h(x) \cdot \tau(x) dx \quad (12)$$

If the travelling wave (3),(4),(5) is not ideal, no symmetrical contact mechanism occurs, see Fig. 1, and

different cases of contact mechanisms have to be distinguished for the torque  $M_R$  (8) and the tangential input power  $p_t$  (12) depending on the sign-function.

1.  $x_{sl} \leq x_0$  and  $x_{sr} \leq x_0$ : As the stick points  $x_{sl}$  and  $x_{sr}$  are located inside the contact region, Three zones have to be considered. In the outer zones frictional forces cause a braking effect; in the intermediate interval a driving action results.
- 2.a)  $x_0 < x_{sl} \leq 2\pi/k - x_0$  and  $-x_0 \leq x_{sr} < x_0$ : Due to a large displacement  $x_c$  the left stick point is outside the contact region. This contact case containing a driving and a slowing zone is presented in Fig. 1.
- b)  $x_{sl} > 2\pi/k - x_0$ : If a wide contact length ( $x_0 > \pi/2$ ) with a "negative" rotor velocity and large  $x_c$  arises, one of the stick points (here  $x_{sl}$ ) shifts in the adjoining contact region (here the left) of the considered region. Thus, in the outer zones driving effects results and in the intermediate interval a slowing action is caused.
- 3.a)  $-x_0 \leq x_{sl} < x_0$  and  $x_0 < x_{sr} \leq 2\pi/k - x_0$ : The counter part to case 2a), where  $x_{sr}$  is located outside.
- b)  $x_{sr} > 2\pi/k - x_0$ : The counter part to case 2b) with  $x_{sr}$  shifts in the right adjoining contact region.
4.  $x_{sl} > x_0$  and  $x_{sr} > x_0$ : The tangential stress  $\tau(x)$  causes only a driving effect (max. driving torque).
- 5.a)  $|v_R| > \hat{v}_h$ : If no stick points  $x_s$  occur, the frictional force affects a slowing down (max. braking torque).
- b)  $x_{sr} < -x_0$  or  $-x_{sl} > x_0$ : Due to a large displacement  $x_c$  in case of small contact length  $x_0$  both stick points are located either on the left or right hand side of the contact mechanism, which causes a braking effect only.

For the diverse contact mechanisms closed form solutions are derived, [4], implemented on the multi-level Simulator SABER as stator/rotor-contact model. Half of the contact length  $x_0$  is determined by evaluation of  $w_R = \hat{w} \cos kx_0$ . For calculation of stick points the term  $d_{sp} v_R = \hat{v}_h(t) \cdot \cos(kx + kx_c)$  of the sign-function has to be solved.

Combining the contact model and the rotor dynamics (9) and (10) we obtain the signal flow diagram of Fig. 2 for analysing of stator/rotor-interaction. The modal forces  $F_{d1}$  and  $F_{d2}$  are the reactions on the stator derived in detail for the total electromechanical system of inverter-fed travelling wave USMs in [4].

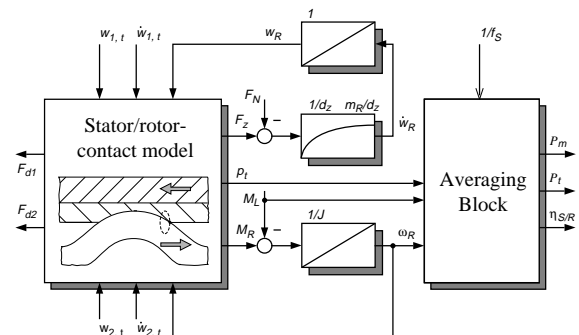


Fig.2: Simulation model for stator/rotor-interface

### Drive Characteristics of travelling wave USMs

For simulation of contact mechanics sinusoidal waveforms are assumed for the modal amplitudes:

$$w_{1,t} = \hat{w}_1 \cdot \sin \omega t, \quad w_{2,t} = \hat{w}_2 \cdot \sin(\omega t + \varphi_m).$$

$\varphi_m$  denotes the temporal phase shift between the waves while  $\hat{w}_1$  and  $\hat{w}_2$  describe their amplitudes, which are equal to  $0,98 \mu\text{m}$  according to the rated operation mode of the drive under study (parameters are scheduled in Table I, see Appendix). For measuring purpose the modal amplitudes are controlled by a suitable experimental set-up, [5],[6]; the feedback information is provided by a two-sensor system, [2].

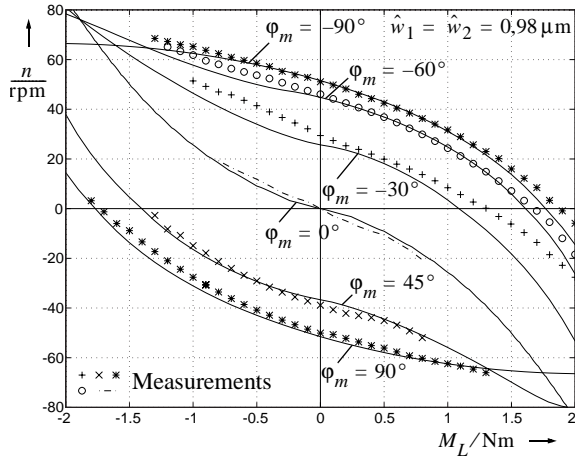


Fig.3: Speed-torque curves of the USM

In Fig. 2 the speed-torque curves are illustrated for the general case of a non ideal travelling wave. For ideal conditions ( $\hat{w}_1 = \hat{w}_2$ ,  $|\varphi_m| = 90^\circ$ ) the highest curve results as expected. With increasing phase deviation from  $|\varphi_m| = 90^\circ$  the curve is lowered. Differing amplitudes ( $\hat{w}_1 \neq \hat{w}_2$ ) result in similar effects, [4], related to the occurring phase shift  $kx_c$ . By adjusting  $\varphi_m$  the drive can be operated in both directions, whereby the speed-torque curve is shifted from one motory quadrant towards the other quadrant. Furthermore non-motory operation modes exist, in which the curves converge to  $M_{R,max} = \pm \mu F_N R_w$ .

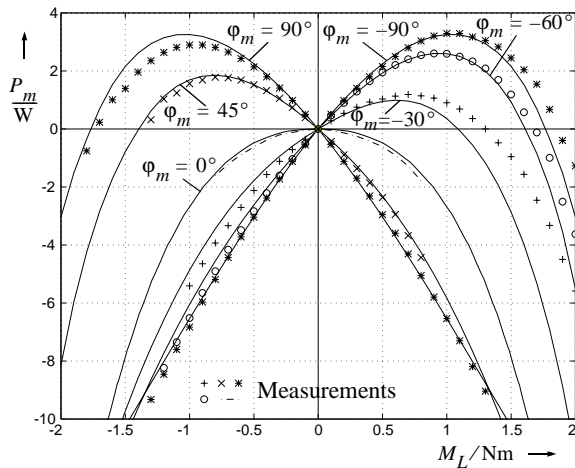


Fig.4: Output power vs torque of the USM

The illustrated measurements verify the contact mechanics approach of the proposed model. There are still some deviations, especially for high loading caused by neglected tangential deformations of contact layer yielding in small stick zones.

In Fig. 2 the resulting curves of mechanical output power  $P_m$  are presented. The maximum power  $P_{m,max} \cong 3,2\text{W}$  is reached in case of  $\overline{M_R} = M_L \cong 1,1\text{Nm}$  and  $|\varphi_m| = 90^\circ$ . For non-ideal waves the power curves drop down significantly and  $P_{m,max}$  is found at a different torque in comparison to ideal conditions.

Non-ideal travelling waves cause a considerable reduction in efficiency. In Fig. 2 the efficiency of the

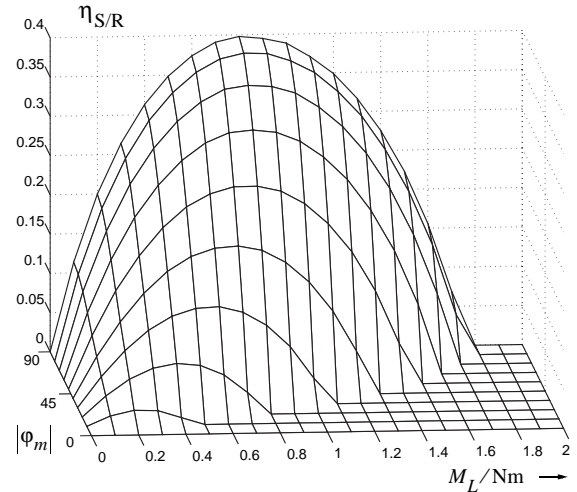


Fig.5: Efficiency of the examined stator/rotor interface

stator/rotor-interface  $\eta_{S/R}$  depending on the torque and phase  $|\varphi_m|$  for constant amplitudes as in Fig. 2 is shown in case of motory operation. Calculating the total efficiency of the drive the losses of the converter, ceramic and stator must be considered. This losses grow approximately quadratic with the amplitude of the electrical and mechanical oscillations. As seen from Fig. 2 an optimized operation mode is obtained in case of ideal conditions. Thus, the variation of the speed-torque characteristic should be implemented by adjusting the wave's amplitude ( $\hat{w}_1 = \hat{w}_2$ ). Furthermore, the maximum torque (power) is never utilized in case of non-ideal conditions, yielding in a reduced operation area.

Due to motor unsymmetries in practice non-ideal travelling waves are generated in case of symmetrical feeding of USMs. Thus measures against unsymmetries are required, which are realized by a novel test set-up for ultrasonic drives, [5],[6].

### Optimization of Stator/Rotor-Contact Interface

The drives characteristics shown before are depending on the construction parameters (see Table I) in general. But for a given motor configuration there is still a questions about an optimized applied axial force  $F_N$ . In order to overcome this, the equations for calculation of mechanical output power  $P_m$  and efficiency  $\eta_{S/R}$  are scheduled for ideal conditions in a normalized form (motory operation mode):

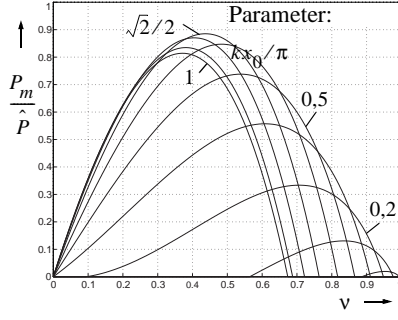


**Fig. 6:** Normalized output power vs speed ratio  $v$  depending on  $kx_0$

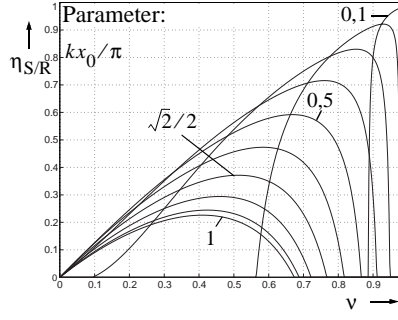


**Fig. 7:** Efficiency vs speed ratio  $v$  depending on  $kx_0$ .

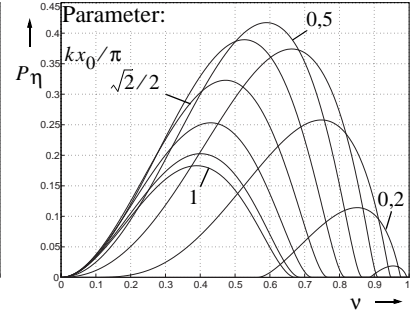


**Fig. 8:** Output power/efficiency vs speed ratio  $v$  depending on  $kx_0$

$$P_m/\hat{P} = 2v(2\sin(\text{acos } v) - 2\text{acos } v \cdot \cos kx_0 - \sin kx_0 + kx_0 \cdot \cos kx_0) , \quad \text{with} \quad \hat{P} = \mu \cdot n \cdot c_N \cdot a \cdot \omega_s \cdot \hat{w}^2 , \quad (13)$$

$$\eta_{S/R} = 2v \frac{2\sin(\text{acos } v) - 2\text{acos } v \cdot \cos kx_0 - \sin kx_0 + kx_0 \cdot \cos kx_0}{2\text{acos } v - kx_0 + \sin(2\text{acos } v) + 1/2 \sin 2kx_0 - 4\cos kx_0 \cdot \sin(\text{acos } v)} , \quad v = \frac{v_R}{\hat{v}_h} = \frac{v_R}{a \cdot \omega_s \cdot k \cdot \hat{w}} . \quad (14)$$

With increasing contact length  $x_0$ , first the normalized output power  $P_m/\hat{P}$  is heightened and after an optimum at  $kx_0 = \sqrt{2}/2 \cdot \pi$  the curves are lowered as seen from Fig. 2. The reason can be explained by the fact that for  $kx_0/\pi < \sqrt{2}/2$  the effect of growing driving zones predominate the effect of increasing braking zones, see Fig. 1. For the prototype drive an axial force of  $F_N = 400\text{N}$  is adjusted. That means, in case of  $\hat{w} = 0,98\mu\text{m}$ , the optimized contact length results (calculated by (9) at steady state). Thus, maximum power is obtained, see Fig. 2 ( $|\phi_m| = 90^\circ$ ).

On the other hand the efficiency illustrated in Fig. 2 is very poor for  $kx_0 \approx \sqrt{2}/2 \cdot \pi$ , yielding in a high wear of the contact layer. Hence, for the selection of an optimized contact length  $x_0$  one has to compromise between a sufficient power curve and a suitable efficiency. Our suggested solution of the multiple optimization problem is to optimize the product of power and efficiency  $P\eta = P_m/\hat{P} \cdot \eta_{S/R}$ .

The resulting curves are presented in Fig. 2. As seen from the illustration the optimum curve is obtained at  $kx_0 = \pi/2$ , which means that only the positive wave hill is in contact with the contact layer. Adjusting this contact length by an optimized axial force  $F_{N, opt} \approx 350\text{N}$  for the rated value of  $\hat{w} = 0,98\mu\text{m}$ , the power in Fig. 2 is lowered only about 18%, but the losses are reduced about 39%. Due to variations of the amplitude  $\hat{w}$  in operation (controlled drive) the axial force  $F_N$  ought to be adapted for optimization discussed above.

## Conclusions

The stator/rotor-interface of USMs is modelled. For optimization of drives performance the speed-torque characteristics as well as the efficiency are analysed in detail and verified by measurements. As a result it is proved that an optimized operation mode is obtained only, if an ideal wave is generated. Finally, design procedures for an optimal choice of the applied axial force are presented. Further investigations concern on the dynamic behaviour [7] and the development of tailored control schemes.

## Acknowledgement

Thanks to the "Deutsche Forschungsgemeinschaft" for financing the project "Wanderwellenantrieb".

## References and Appendix

- [1] T. Sashida, T. Kenjo: "An introduction to ultrasonic motors", Clarendon Press - Oxford (1993).
- [2] P. Hagedorn, J. Wallaschek: Travelling wave ultrasonic motors, part I: "Working principle and mathematical modelling of the stator". Journal of Sound and Vibration (1992), 155(1), pp. 31-46.
- [3] S. Furuya et al: "Load-adaptive frequency tracking control implementation of two-phase resonant inverter for ultrasonic motor." IEEE Transactions on Power Electronics, Vol. 7, 1992, pp. 542-550.
- [4] J. Maas et al: "Simulation Model for Ultrasonic Motors powered by Resonant Converters". IAS'95, Orlando (USA), pp. 111-120, Oct. 1995.
- [5] J. Maas et al: "Prototype drive and modulation concepts for DSP-controlled ultrasonic motors powered by resonant converters." EPE'95, Sevilla (Spain), pp. 1777-1782, Sept. 1995.
- [6] J. Maas, H. Grotstollen: "Beitrag zur Systemoptimierung eines geregelten Ultraschall-Wanderwellenantriebs". Fachtagung Leistungselektro. Aktoren und intell. Bewegungssteuer., Magdeburg, pp. 213-222, March 1996.
- [7] J. Maas, P. Ide, H. Grotstollen: "Dynamic Analysis of Inverter-Fed Ultrasonic Motors." PESC'96, Baveno (Italy), June 24.-27. 1996.

TABLE I  
Parameters of stator/rotor-interface

Parameter	Description	Value
$n$	Number of nodal diameters	11
$a$	Surface distance	4.5 mm
$c_N/k$	Stiffness of contact layer	8950 N/mm
$R_w$	Average radius of contact area	44 mm
$F_N$	Axial force applied to the rotor	400 N
$\mu$	Coulomb's friction coefficient	0.12